Revision 1

Arsenate Partitioning from Ferrihydrite to Hematite: Spectroscopic Evidence

[1]Soumya Das*, [1]Joseph Essilfie-Dughan, and [1]M. Jim Hendry

[1]Department of Geological Sciences, University of Saskatchewan, 114 Science Place
Saskatoon, SK S7N 5E2, CANADA

* Corresponding author: Tel: 306-966-4664; fax: 306-966-8593
E-mail address: sod671@campus.usask.ca

For submission to American Mineralogist 2013

ABSTRACT

Despite the number of detailed studies on arsenate adsorption onto synthetic 2-line ferrihydrite carried out during the past few decades, questions remain regarding the fate of adsorbed arsenate during phase transformation of this poorly crystalline iron oxy-hydroxide. We assessed arsenate partitioning during this transformation by aging synthetic 2-line ferrihydrite with adsorbed arsenate (at an As/Fe molar ratio of ~0.017) for 7 d at 75 °C under highly alkaline conditions (pH ~10). X-ray diffraction patterns show that ~55% of the ferrihydrite converted almost entirely to hematite (with traces of goethite) after aging 7 d, accompanied by a ~54% loss of reactive surface area (BET). ICP-MS analyses indicate that despite this conversion and significant loss of surface area, the aqueous arsenate concentration decreased from ~1.48 to ~0.51 mg/L during the course of the experiment. XAS analyses suggest that the concentration of arsenate and its speciation are controlled by its incorporated into the hematite.

Key words: Ferrihydrite, Hematite, Arsenic, Structural Incorporation

INTRODUCTION

Arsenic contamination in both waters and soils and the associated health hazards are a global concern (Vaughan 2006). Although arsenic concentrations in natural waters are usually low (1-10 μg/L) (Smedley and Kinniburgh 2002), high levels of arsenic in both surface and groundwaters are reported in North America, Asia, Europe, and Africa (Vaughan 2006). In addition, exceptionally high concentrations (50-350 mg/L) of arsenic are reported for effluents generated by mining and metallurgical operations (Smedley and Kinniburgh 2002; Morin and Calas 2006; Vaughan 2006). Owing to its toxicity, particularly its carcinogenicity, the World Health Organization (WHO) reduced the maximum permissible level in drinking water from 50 to 10 μg/L in 1993 (WHO 1993). Likewise, the United Stated Environmental Protection Agency (US EPA) revised their drinking water standards from 50 to 10 μg/L in 2001 (US EPA 2001).

Adsorption onto natural oxides, more specifically iron oxides, can control the speciation and aqueous concentration of contaminants, including arsenic, in natural waters (Smedley and Kinniburgh 2002). Among all iron oxides and hydroxides, amorphous iron oxy-hydroxide or 2-line ferrihydrite (hereafter called ferrihydrite) is the most common and important adsorbent for contaminants in natural soils and sediments (Michel et al. 2007). Owing to its ubiquity, high surface area, and reactivity, ferrihydrite can play a major role in contaminant speciation in natural and process waters (Michel et al. 2007) and has thus captured the recent attention of the geo-scientific community, reflected in an overwhelming number of studies on contaminant adsorption onto ferrihydrite (Pierce and Moore 1982; Waychunas et al. 1996; Wilkie and Hering 1996; Jain et al. 1999; Jia and Demopoulos 2005). Under oxic conditions, ferrihydrite is metastable and transforms to more stable and crystalline phases, such as goethite and/or hematite, depending upon pH and temperature (Cudennec and Lecerf 2006). However, the

presence of solutes such as arsenate can limit this transformation process at very high As/Fe molar ratios (0.500, 0.100, 0.050) under alkaline conditions (Das et al. 2011a). At lower As/Fe ratios (achieved either by adsorption or co-precipitation), this transformation process slows drastically even under highly alkaline conditions (pH 10-12), and the transformation product is dominated by hematite (Paige et al. 1996; Das et al. 2011a). This transformation also leads to a substantial loss of reactive surface area (Das et al. 2011b), which could eventually trigger the release of adsorbed arsenate from the surface of ferrihydrite under alkaline conditions. Thus, the ability and retention capability of the newly formed solid (hematite) for arsenate requires investigation. Moreover, the fate of adsorbed arsenate, including its release from the solid phase or re-adsorption/structural incorporation into newly formed solids, has been neglected in studies to date. Thus, this study evaluated the fate of arsenate adsorbed onto ferrihydrite during aging. Aging was conducted on freshly prepared ferrihydrite under highly alkaline (pH ~10) conditions (to minimize adsorption), at elevated temperature (75 °C) (to expedite the transformation), and with a moderate As/Fe molar ratio (~0.017; to allow transformation) achieved via adsorption. Samples (control and aged) were analyzed via X-ray diffraction (XRD), surface area analyses (BET), inductively coupled plasma mass spectrometry (ICP-MS), and X-ray absorption spectroscopic (XAS) techniques. The results are relevant with respect to the environmental fate of arsenic previously adsorbed onto ferrihydrite, and may shed light on the fate of other elements of concern (EOCs), during ferrihydrite phase transformation in a variety of environmental settings.

MATERIALS AND METHODS

All synthetic solids, namely 2-line ferrihydrite, goethite, and hematite, were prepared according to the methods of Schwertmann and Cornell (1991). In brief, 2-line ferrihydrite was synthesized (with slight modification) by titrating anhydrous $FeCl_3$ solution (instead of ferric nitrate) with 1M NaOH (instead of 1M KOH) to a pH of 7-8. Goethite was synthesized by aging freshly prepared 2-line ferrihydrite under highly alkaline conditions (by addition of 5M KOH) for 60 h at 70 °C in a water bath. Finally, hematite was synthesized by heating an $Fe(NO_3)_3 \cdot 9H_2O$ solution in a water bath at 98 °C for 7 d. All synthesized solid precipitates were then washed 4-5 times with double distilled deionized water (DDI) by a pressure filter to remove any salt impurities. The Raman spectrum of the synthesized ferrihydrite (data not presented) did not show any additional band positions indicative of the presence of chloride ions. Thus, the synthetic ferrihydrite was assumed to be relatively free of chlorides that could interfere during the transformation process. All of these synthesized wet precipitates were then freeze-dried and refrigerated until further analyses.

Freshly prepared ferrihydrite precipitate was re-suspended (never dried) in 200 mL of DDI water in a polyethylene bottle and homogenized by stirring on a stir plate at room temperature for ~30 min. Solid hydrated sodium arsenate ($Na_2HAsO_4 \cdot 7H_2O$) was added to the homogenized slurry under continued stirring to generate arsenate adsorbed to 2-line ferrihydrite at an As/Fe molar ratio of ~0.017. The pH of the slurry was raised to pH ~10 by adding trace metal grade NaOH (0.1 or 0.01M as needed) using a 10 μL pipette. To ensure complete homogenization, the slurry was kept on the stir plate with constant stirring for nearly 1 h. The pH was then re-measured and a ~25 mL slurry sample taken and centrifuged; the supernatant was removed and stored in a refrigerator for ICP-MS analysis. A portion of the wet ferrihydrite precipitate was scooped by spatula and transferred to a separate centrifuge tube and kept in the refrigerator as a

wet paste for analysis via XAS. The remainder of the precipitate was then freeze-dried and refrigerated for subsequent XRD, BET, and ICP-MS analyses. These samples served as t=0 or control samples (arsenate sorbed onto ferrihydrite). Subsequently, the polyethylene bottle containing the ferrihydrite slurry was capped tightly and transferred to a water bath preheated to 75(±2) °C. The pH was measured after 2, 3, 4, 5, 6, and 7 d and maintained at ≥ 9.6 throughout the experiment by addition of 0.01M NaOH as needed. Samples were collected from the slurry after 2, 3, 4, 5, 6, and 7 days and processed as for the t=0 sample. All XRD, BET, and ICP-MS analyses were conducted within 7 d and XAS was conducted within 15 d of sample collection.

XRD analyses were performed on all freeze-dried, ground (using mortar and pestle to break up any larger aggregates), solid samples (control and transformed phases) using a PANanalytical Empyrean X-ray diffractometer equipped with a Spellman generator and Co X-ray tube set to 40 kV and 45 mA. The instrument was configured with an incident beam path Fe β-filter and 1 degree anti-scatter slit, 0.02 mm Soller slits, and divergence and receiving slits fixed at 0.5 degrees. Dried samples were mounted on a glass plate and run using a spinning reflection/transmission stage. Spectra were acquired from 10 to 80 degrees with a step size of 0.0167 degrees and a scan speed of 1 degree/min. All raw data files were converted to Excel files and the resulting spectra plotted as intensity versus 2θ.

In addition to the XRD analyses of the control and transformed phases, XRD scans were also performed on pre-determined mixtures of pure ferrihydrite and goethite (1-90 wt%) and pure ferrihydrite and hematite (1-90 wt%) for quantification purposes using the methods described by Das et al. (2011a) with slight modification. The intensities of the individual XRD scans of the transformation products were then calibrated against the XRD scans from the pre-

137 determined mixtures using the integrated intensities. Using this method, the lower limit of
138 detection of both goethite and hematite was 1 wt% with an accuracy of ±5 wt%.

139 Surface area measurements were conducted on five freeze-dried, ground, solid samples
140 (control and transformed samples at 0, 3, 5, 6, and 7 d) via 11-pt BET-nitrogen isotherms using a
141 Quantachrome NOVA 2200e Surface Area and Pore Size Analyzer to evaluate changes in
142 reactive surface areas during aging. Samples were degassed at 80 °C for 24 h prior to any
143 analyses. The multi-point BET surface areas were then measured at atmospheric pressure, and
144 the adsorption isotherms achieved at a p/p_o range of 0.05-0.35.

145 Solid, freeze-dried, ground samples (0, 2, 3, 4, 5, 6, and 7 d) were analyzed via ICP-MS
146 (Perkin Elmer NexIon 300D ICP-MS) to evaluate the partitioning of arsenic onto the solid
147 phases during ferrihydrite phase transformation. In brief, dried and ground solid samples (~100
148 mg) were digested in ~5 mL of double distilled concentrated HF (48-51%) in Teflon® jars to
149 which ~5 mL of double distilled concentrated (16N) HNO_3 were then added. All Teflon® jars
150 were then capped tightly and heated to ~100-150 °C for 3 d. The jars were then cooled to room
151 temperature, then 1-2 mL of concentrated HNO_3 and 1-2 mL of HF added. The solutions were
152 refluxed for 3 d to ensure dissolution of the solid precipitates. Lids were removed and rinsed
153 three times with a few mL of 16N HNO_3 to remove any sample residues and then evaporated to
154 dryness. Subsequently, 2.5 mL of 8N HNO_3 and 0.5 mL H_2O_2 were added to the jars, which were
155 covered and warmed gently to dissolve any undigested residues. The lids were then rinsed for a
156 final time with Milli-Q water and all samples transferred to sample bottles, which were made up
157 to a final weight of 100 g by addition of Milli-Q water for analysis via ICP-MS.

158 ICP-MS analyses of the aqueous samples (supernatants after centrifugation) for 0, 2, 3, 4, 5,
159 6, and 7 d were performed via a Perkin Elmer NexIon 300D ICP-MS to define the partitioning of

arsenic in the aqueous phase during aging. Briefly, a known volume of aqueous sample was mixed with a known volume of standards before analysis. Indium was used as an internal standard to overcome any matrix effects and also to avoid any signal drift with time.

Two solid samples (0 and 7 d) were analyzed via XAS to evaluate the change in the bonding environment of arsenate during the phase transformation of ferrihydrite. Both samples were loaded onto Kapton® tape as a wet paste over a Teflon® sample holder. Arsenic K-edge XAS spectral data were collected on each sample at ambient temperature and pressure using the Hard X-ray Microanalysis beamline (HXMA - 06ID-1) at the Canadian Light Source (University of Saskatchewan), a third-generation synchrotron facility operating at an electron energy of 2.9 GeV and injection current of ~250 mA. The synchrotron source at the HXMA beamline is a superconducting wiggler equipped with a double-crystal Si(111) monochromator and Rh-coated collimating mirror. The beam was detuned at approximately 50% to reject higher-order harmonic frequencies and to prevent detector saturation. X-ray absorption spectra were collected from –200 to +800 eV at the K-edge of As (11,867 eV). The monochromator step size was reduced to 0.5 eV in the X-ray absorption near-edge spectroscopy (XANES) region and 0.05 Å in the extended X-ray absorption fine structure (EXAFS) region. To aid the characterization of change in the bonding environment of arsenate during the phase transformation of ferrihydrite, XAS data were also collected on scorodite ($FeAsO_4.2H_2O$) and arsenate adsorbed on hematite. All data were collected in fluorescence mode using 32-element solid-state germanium with simultaneous measurement of Au reference spectra for energy calibration of each sample spectra. Three XAS scans were collected for each sample and averaged to increase the signal-to-noise ratio.

The XAS data were analyzed using IFFEFIT (ATHENA & ARTEMIS) (Ravel and Newville 2005). ATHENA was used for data reduction, which included the standard procedures of energy

calibration, averaging of multiple scans, background subtraction, per atom normalization, and extraction of the EXAFS whereas ARTEMIS was used for EXAFS data analysis of the As spectra. The k^3-weighted $\chi(k)$ function $[\chi(k)k^3]$ in k-space ($Å^{-1}$) was Fourier transformed (FT) to produce the radial structure function (RSF) in R-space (Å) using a k-range of approximately 3-13 $Å^{-1}$. The $\chi(k)k^3$ in k-space ($Å^{-1}$) and FT RSF in R-space (Å) of the As K-edge of both samples were all fitted with *ab initio* phase and amplitude functions generated with FEFF version 6L that comes with the IFFEFIT package (Rehr et al. 1992).

The XANES region of the XAS spectra provides information about the oxidation state as well as the coordination environment (geometrical arrangement of atoms) of the absorber atom (i.e., As) (Kelly et al. 2008). Thus, to test the hypothesis of potential reduction in the oxidation state of As upon adsorption onto ferrihydrite (day 0) as well as during the transformation of ferrihydrite to hematite (day 7), the normalized As XANES spectra were compared to reference compounds (sodium arsenite and sodium arsenate) of known oxidation state (+3 and + 5, respectively).

A kinetic fit of the % hematite formed as well as the amount of ferrihydrite remaining as a function of time during aging were obtained using Sigmaplot ® (Fig. 3). The fit shows that the rate of ferrihydrite transformation to hematite follows first order kinetics according to:

$$[A]_t = [A]_0 e^{-kt}, \quad (1)$$

where $[A]_t$ is the amount of ferrihydrite remaining at time t, $[A]_0$ is the initial amount of ferrihydrite before phase transformation, k is a rate constant, and t is time.

RESULTS AND DISCUSSION

Characterization and quantification of iron oxide/hydroxide during aging

Synthetic iron oxide and oxy-hydroxide precipitates were characterized via XRD to ensure purity (Fig. 1). All significant peaks on the XRD scans closely matched previous reports (Schwertman and Cornell 1991). XRD scans of transformed samples reveal that transformation starts on day 2 and the only transformation product is hematite (Fig. 2). All characteristic hematite peaks, such as at 2θ of ~28, 38, 42, 48, 52, 58, 64, 68, 74, and 76°, corresponding to crystallographic planes of (012), (104), (110), (113), (202), (024), (116), (018), (214), and (300), respectively (Schwertman and Cornell 1991), grew and developed as the aging continued from day 2 to 7 (Fig. 2). However, an additional minor peak appeared on day 6, at a 2θ of ~25, and remained at a similar intensity until day 7. This peak was identified as the (110) peak of goethite (Fig. 2). No other major or minor peaks of any other phases were identified. These findings are in excellent agreement with previously published results (Paige at al. 1996; Das et al. 2011a) that indicate hematite is the dominant product during ferrihydrite transformation under alkaline conditions (pH ~10-12) and the influence of either adsorbed or co-precipitated arsenate. Quantification via integrated intensities calculated from the XRD scans demonstrate that ~5, 7, 14, 24, 38, and 55% of the ferrihydrite converted to hematite by 2, 3, 4, 5, 6, and 7 d, respectively (Table 1). This transformation process leads to a substantial loss of reactive surface area, from ~241 to ~112 m^2/g (Table 1) for a net reduction of ~54%. The kinetics of this transformation can be satisfactorily fitted using the first order rate law equation that is consistent with previous reports on the transformation of ferrihydrite to hematite in the presence of adsorbed arsenate (Das et al. 2011a) (Fig. 3).

Arsenate partitioning during ferrihydrite transformation

The initial pH of the slurry prepared for the aging process was 10.03. However, after 1 d of aging the pH decreased to 9.03; this was readjusted to 9.93 with the addition of a few drops of

0.01 M NaOH. Another decrease in pH, to 9.57, occurred on 3 d, and was again readjusted to 9.85 with 0.01M NaOH. Interestingly, no further decrease in pH was noted; instead, the pH of the slurry increased from 9.85 to 9.88, 10.10, and 10.56 after 5, 6, and 7 d, respectively. The significant loss of reactive surface area, along with the rising pH of the slurry (from 10.03 on day 0 to 10.56 on day 7) could trigger a release of adsorbed arsenate from ferrihydrite surfaces during aging. Surprisingly, aqueous ICP-MS analyses illustrate a different perspective with respect to arsenate partitioning. The aqueous As concentration on 0 d was 1.48 mg/L and increased by day 2 to 2.28 mg/L (Table 1), indicating the release of some arsenate from the ferrihydrite surface. However, as aging continued (with consequent increases in percent hematite formation and associated reduction in specific surface area), the aqueous As concentration decreased from 2.28 to 1.92, 1.81, 1.54, 1.11, and 0.51 mg/L after 3, 4, 5, 6, and 7 d, respectively (Table 1). This decrease in aqueous As concentration in the system cannot be explained by re-adsorption onto hematite as discussed earlier, because the surface area decreased as the transformation of ferrihydrite to hematite proceeded. The only mechanism that can lead to this continuous decrease of aqueous arsenate is the structural incorporation of arsenate into the newly formed hematite. This observation is supported by solid ICP-MS results that show increasing As concentrations in the solid phase and thus an increase the As/Fe ratio from 0.016 on 0 d to 0.018 on 7 d. Specifically, aqueous arsenate was incorporated into the hematite structure, which formed upon transformation from ferrihydrite over time, resulting in a decrease in the aqueous As concentration.

Evidence of structural incorporation via XAS analyses

To test this hypothesis of structural incorporation, and for further clarification of the ICP-MS results, XAS spectroscopy was conducted on two solid samples (0 and 7 d). The XANES

spectra for As in both samples match the edge position of the As^{+5} standard ($Na_2HAsO_4.7H_2O$) (Fig. 4a), assuming that the oxidation state of As is preserved during adsorption onto ferrihydrite as well as during the transformation of ferrihydrite to hematite. XANES is also sensitive to the coordination environment (geometrical arrangement of atoms) of the absorber atom (George and Pickering 2007; Kelly et al. 2008). Although an overlap comparison of the normalized day 0 and day 7 XANES spectra shows a flattening of spectral features (as indicated by the arrow in Fig. 4a), suggesting a possible change in the coordination environment of As during transformation of ferrihydrite to hematite, this is not conclusive evidence.

To further probe the coordination environment of As during ferrihydrite transformation to hematite, EXAFS spectra of both samples were collected to obtain critical information (i.e., bond distances, bonded atoms, coordination numbers) about the absorber atom (McNear et al. 2005). Figures 4b and 4c show the $\chi(k)k^3$ in k-space ($Å^{-1}$) and Fourier transform radial structure function (FT RSF) in R-space (Å) of the day 0 sample (arsenate adsorbed on ferrihydrite) and the day 7 sample (arsenate incorporated into hematite formed from the ferrihydrite transformation), respectively. The observed k-space spectra are attributed to the backscattering associated with the nearest bonded oxygen atoms (i.e., As–O shell), and the presence of the shoulders and peak splitting on the wave pattern is attributed to backscattering from distant bonded atoms (i.e., As–Fe shell). Conspicuous on the day 7 k-space spectra is a split peak between 4 and 5 $Å^{-1}$ as well as spectral features between 12 and 13 $Å^{-1}$ (indicated by arrows). This is in contrast to the k-space spectra in these regions for the day 0 sample, where the region flattens out and is consistent with previously published EXAFS studies on arsenate adsorbed on ferrihydrite (Foster et al. 1998; Moldovan et al. 2003; Paktunc et al. 2004, 2008; Chen et al. 2009). The observed differences are more evident in the FT in R-space (Å) (Fig. 4c), which can provide estimates of bond distances

between the central absorber atom (As) and its nearest neighbours. The first and the most pronounced peak in the FT R-space is at ~1.5 Å (uncorrected for phase shifts) for both samples, and represents the scattering from oxygen atoms directly bonded to the As atom. The second peak in the day 0 FT R-space at ~3.0 Å (uncorrected for phase shifts) corresponds to As–Fe bonding. However, the day 7 FT R-space contains second and third peaks at ~2.7 and ~3.25 Å, respectively, both of which correspond to As–Fe bonding. This suggests the coordination environment of the adsorbed arsenate changed upon transformation of the ferrihydrite to hematite.

Quantitative non-linear least square fit analysis of the calculated *ab initio* phase and amplitude functions (using FEFF 6L) to the $\chi(k)k^3$ in k-space ($Å^{-1}$) and FT RSF in R-space (Å) (Fig. 5a, Table 2) indicates that the first shell (As–O) in both samples has a coordination number (CN) of 4 and an average As–O bond distance of 1.69 ± 0.02 Å. In both samples, the CN and bond lengths correspond to a tetrahedral coordination of the oxygen atoms around the As. This is in excellent agreement with published EXAFS analysis of arsenate (AsO_4^{3-}) (Moldovan et al. 2003; Chen et al. 2009; Essilfie-Dughan et al. 2013). The results of the fit analyses indicate that the second shell (As–Fe) of the day 0 sample has a CN of 2.0 with an average bond distance of 3.27 ± 0.02 Å, which is typical of arsenate adsorbed on ferrihydrite via bidentate binuclear bridging (Waychunas et al. 1993; Moldovan et al. 2003; Foster 2003; Chen et al. 2009) as illustrated in Figure 2b (day 0). However, the second (As–Fe1) and third (As–Fe2) shells of the day 7 sample have CNs of 1.1 and 1.9 and average bond distances of 2.83 ± 0.02 and 3.36 ± 0.02 Å, respectively. The As–Fe1 bond length of 2.83 and CN of 1.1 indicate that the arsenate tetrahedron is bonded to an edge sharing ferric iron octahedral through a bidentate-mononuclear complex (Fendorf et al. 1997; Ladeira et al. 2001), whereas the As–Fe2 bond length of 3.36 and

298 CN of 1.9 indicate that the arsenate tetrahedron is bonded to two ferric iron octahedra through a
299 bidentate binuclear corner-sharing complex (Foster 2003; Sherman and Randall 2003; Wang and
300 Mulligan 2008), as illustrated in Figure 5b (day 7). These results suggest that arsenate adsorbed
301 onto ferrihydrite during the transformation to hematite does not merely remain adsorbed on the
302 surface, but is incorporated into the hematite structure via both a bidentate-mononuclear complex
303 and a bidentate binuclear corner-sharing complex. The above description of the coordination
304 environment of arsenate incorporated into the hematite structure is different than the fit analysis
305 based on As K-edge EXAFS spectra of arsenate adsorbed on hematite (Figure 5 & Table 2),
306 which indicates two shells. The first coordination shell (As–O) with a bond distance of 1.69 Å
307 and a CN of 4 is consistent with the tetrahedral molecular structure of arsenate as described
308 above, but the second coordination shell (As–Fe) with a bond distance of 2.83 Å and a CN of 0.9
309 indicates the arsenate is adsorbed onto the hematite through a bidentate mononuclear complex
310 (Fendorf et al. 1997; Ladeira et al. 2001; Arai et al. 2004). Similarly, the fit analysis based on the
311 As K-edge EXAFS spectra (Figure 5 & Table 2) shows that the coordination environment of
312 arsenate incorporated into the hematite structure during the phase transformation is different
313 from that of scorodite (a common ferric arsenate mineral). Scorodite has the typical tetrahedral
314 first coordination As–O shell at an average bond distance of 1.68 Å but also a second As–Fe
315 shell with a CN of 4.0 and an average bond distance of 3.35 Å; this indicates that the scorodite
316 local structure is highly symmetrical and made up of the arsenate tetrahedron coordinated with
317 four ferric iron octahedra (Foster 2003; Moldovan et al. 2003; Chen et al. 2009). The differences
318 in the As–Fe shell results for the three arsenic-iron mineral phases described above suggest that
319 they have considerably different local structures.
320

ENVIRONMENTAL SIGNIFICANCE

Attention given to ferrihydrite during last few decades is due to its ubiquity, high surface reactivity, and ability to adsorb trace contaminants in a narrow pH range. This adsorption mechanism is thought to be a driving process in contaminant sequestration in the environment and, thus, most ferrihydrite-related studies focus on this aspect. However, the current study demonstrates that structural incorporation may be preferable to adsorption for trace metal partitioning during ferrihydrite phase transformation. More importantly, such structural incorporation appears to be independent of the reactive surface areas of the incorporating sorbent. With further evidence and studies focused on other trace contaminants, this structural incorporation mechanism might lead to a new understanding of trace metal partitioning in the environment and possible applications to a wide range of environmental conditions.

Acknowledgements

The authors acknowledge the assistance of Tom Bonli with XRD analyses, Erin Schmeling with BET analyses, and Jianzhong Fan with ICP-MS analyses. Funding was provided by the Natural Sciences and Engineering Research Council of Canada (NSERC) Industrial Research Chair program and Cameco Corporation (MJH).

References

Arai, Y., Sparks, D.L., and Davis, J.A. (2004) Effects of dissolved carbonate on arsenate adsorption and surface speciation at the hematite-water interface. Environmental Science and Technology, 38, 817-824.

Chen, N., Jiang, D.T., Cutler, J., Kotzer, T., Jia, Y.F., Demopoulos, G.P., and Rowson, J.W. (2009) Structural characterization of poorly-crystalline scorodite, iron(III)-arsenate co-precipitates and uranium mill neutralized raffinate solids using X-ray absorption fine structure spectroscopy. Geochimica et Cosmochimica Acta, 73, 3260-3276.

Cudennec, Y., and Lecerf, A. (2006) The transformation of ferrihydrite into goethite or hematite, revisited. Journal of Solid State Chemistry, 179, 716-722.

Das, S., Hendry, M.J., and Essilfie-Dughan, J. (2011a) Effects of adsorbed arsenate on the rate of transformation of 2-line ferrihydrite at pH 10. Environmental Science and Technology, 45, 5557-5563.

Das, S., Hendry, M.J., and Essilfie-Dughan, J. (2011b) The transformation of two-line ferrihydrite to goethite and hematite as a function of pH and temperature. Environmental Science and Technology, 45, 268-275.

Essilfie-Dughan, J., Hendry, M.J., Warner, J., and Kotzer, T. (2013) Arsenic and iron speciation in uranium mine tailings using X-ray absorption spectroscopy. Applied Geochemistry, 28, 11-18.

Fendorf, S., Eick, M.J., Grossl, P., and Sparks, D.L. (1997) Arsenate and chromate retention mechanisms on goethite. 1. surface structure. Environmental Science and Technology, 31, 315-320.

Foster, A.L., Brown, G.E., Tingle, T.N., and Parks, G.A. (1998) Quantitative arsenic speciation in mine tailings using X-ray absorption spectroscopy. American Mineralogist, 83, 553-568.

Foster, A.L. (2003) Spectroscopic investigations of arsenic species in solid phases. In: Welch, A. H., Stollenwerk, K. G. (eds.) Arsenic in Ground Water: Geochemistry and Occurrence, Kluwer Academic Publishers, Dordrecht.

George, G.N., and Pickering, I.J. (2007) X-ray absorption spectroscopy in biology and chemistry. NATO Advanced Science Institutes Series B: Physics. Plenum, New York, 97-119.

Jain, A., Raven, K.P., and Loeppert, R.H. (1999) Arsenite and arsenate adsorption on ferrihydrite: surface charge reduction and net OH^- release stoichiometry. Environmental Science and Technology, 33, 1179-1184.

Jia, Y., and Demopoulos, G.P. (2005) Adsorption of arsenate onto ferrihydrite from aqueous solution: influence of media (sulfate vs. nitrate), added gypsum, and pH alteration. Environmental Science and Technology, 39, 9523-9527.

Kelly, S.D., Hesterberg, D., and Ravel, B. (2008) Analysis of soils and minerals using X-ray absorption spectroscopy. In: Ulrey, A. L.; Drees, L. R. (eds) Soil Science Society of America (Eds.), Methods of soil analysis. Part 5, Mineralogical methods. Soil Science Society of America, Madison, WI.

Ladeira, A.C.Q., Ciminelli, V.S.T., Duarte, H.A., Alves, M.C.M., and Ramos, A.Y. (2001) Mechanism of anion retention from EXAFS and density functional calculations: arsenic (V) adsorbed on gibbsite. Geochimica et Cosmochimica Acta, 65, 1211-1217.

McNear, D.H., Tappero, R., and Sparks, D.L. (2005) Shining light on metals in the environment. Elements, 1, 211-216.

Michel, F.M., Ehm, L., Antao, S.M., Lee, P.L., Chupas, P.J., Liu, G., Strongin, D.R., Schoonen, M.A.A., Phillips, B.L., and Parise, J.B. (2007) The structure of ferrihydrite, a nanocrystalline material. Science, 316, 1726-1729.

Moldovan, B.J., Jiang, D.T., and Hendry, M.J. (2003) Mineralogical characterization of arsenic in uranium mine tailings precipitated from iron-rich hydrometallurgical solutions. Environmental Science and Technology, 37, 873-879.

Morin, G., and Calas, G. (2006) Arsenic in soils, mine tailings, and former industrial sites. Elements, 2, 97-101.

Paige, C.R., Snodgrass, W.J., Nicholson, R.V., and Scharer, J.M. (1996) The crystallization of arsenate-contaminated iron hydroxide solids at high pH. Water Environment Research, 68, 981-987.

Paktunc, D., Foster, A., Heald, S., and Laflamme, G. (2004) Speciation and characterization of arsenic in gold ores and cyanidation tailings using X-ray absorption spectroscopy. Geochimica et Cosmochimica Acta, 68, 969-983.

Paktunc, D., Dutrizac, J., and Gertsman, V. (2008) Synthesis and phase transformations involving scorodite, ferric arsenate and arsenical ferrihydrite: implications for arsenic mobility. Geochimica et Cosmochimica Acta, 72, 2649-2672.

Pierce, M.L., and Moore, C.B. (1982) Adsorption of arsenite and arsenate on amorphous iron hydroxide. Water Research, 16, 1247-1253.

Ravel, B., and Newville, M. (2005) ATHENA, ARTEMIS, HEPHAESTUS: data analysis for X-ray absorption spectroscopy using IFEFFIT. Journal of Synchrotron Radiation, 12, 537-541.

Rehr, J.J., Albers, R.C., and Zabinsky, S.I. (1992) High-order multiple-scattering calculations of X-ray-absorption fine structure. Physical Review Letters, 69, 3397- 3400.

Schwertmann, U., and Cornell, R.M. (1991) Iron oxides in the laboratory. VCH, Weinheim, Germany.

Sherman, D.M., and Randall. S.R. (2003) Surface complexation of arsenic(V) to iron(III) (hydr)oxides: structural mechanism from ab initio molecular geometries and EXAFS spectroscopy. Geochimica et Cosmochimica Acta, 67, 4223-4230.

Smedley, P.L., and Kinniburgh, D.G. (2002) A review of the source, behaviour and distribution of arsenic in natural waters. Applied Geochemistry, 17, 517-568.

U.S. EPA (2001) Fact sheet: Drinking water standard for arsenic, EPA, Washington, D.C.

Vaughan, D.J. (2006) Arsenic. Elements, 2, 71-75.

Wang, S., and Mulligan, C.N. (2008) Speciation and surface structure of inorganic arsenic in solid phases: a review. Environmental International, 34, 867-879.

Waychunas, G.A., Rea, B.A., Fuller, C.C., and Davis, J.A. (1993) Surface chemistry of ferrihydrite: part 1. EXAFS studies of the geometry of coprecipitated and adsorbed arsenate. Geochimica et Cosmochimica Acta, 57, 2251-2269.

Waychunas, G.A., Fuller, C.C., Rea, B.A., and Davis, J.A. (1996) Wide angle x-ray scattering (WAXS) of "two-line" ferrihydrite structure: Effect of arsenate sorption and counterion variation and comparison with EXAFS results. Geochimica et Cosmochimica Acta, 60, 1765-1781.

WHO (1993) Guidelines for drinking water quality, vol. 1: Recommendations, 2nd ed. WHO, Geneva.

Wilkie, J.A., and Hering, J.G. (1996) Adsorption of arsenic onto hydrous ferric oxide: effects of adsorbate/adsorbent ratios and co-occurring solutes. Colloids and Surfaces A, 107, 97-110.

Figure captions

Fig.1. XRD scan of pure iron oxide and oxy-hydroxide phases: (a) 2-line ferrihydrite, (b) goethite, and (c) hematite.

Fig. 2. XRD scans of 2-line ferrihydrite aging experiments at (a) 0, (b) 2, (c) 3, (d) 4, (e) 5, (f) 6, and (g) 7 d. Aging was conducted for 7 d at 75 °C and at pH ~10. G and H signify goethite and hematite peaks, respectively.

Fig. 3. Reaction kinetics of ferrihydrite transformation and subsequent hematite formation in the presence of adsorbed arsenate. Aging was conducted at 75 °C for 7 d. Both ferrihydrite transformation and hematite formation follow first order reaction kinetics under alkaline conditions.

Fig. 4. (a) As K-edge X-ray absorption near-edge spectra (XANES) for day 0 (arsenate adsorbed on ferrihydrite), day 7 (arsenate incorporated into hematite formed from the ferrihydrite transformation), and reference compounds with As oxidation states of +3 (arsenite) and +5 (arsenate), (b) As K-edge k^3-weighted EXAFS spectra, and (c) Fourier transform (FT) spectra for a k interval of 3-13$Å^{-1}$ for day 0 and day 7. The first major peak in the FT spectra is from the nearest neighbor As–O shell and the second major peak is mainly from the As–Fe shell. However, day 7 has two As–Fe peaks (As-Fe1 and As-Fe2). The Fourier transformed spectra have not been corrected for phase shift.

Fig. 5 (a) Quantitative non-linear least square fit analysis of the calculated *ab initio* phase and amplitude functions of the As EXAFS spectra at day 0 and day 7 in R-space as well that of arsenate adsorbed on ferrihydrite and scorodite. (b) Surface structure binding illustration of arsenic adsorbed to ferrihydrite via a bidentate binuclear corner-sharing complex (day 0) and arsenate incorporated into hematite formed from the transformed ferrihydrite via both a bidentate-mononuclear complex and a bidentate binuclear corner-sharing complex (day 7).

476 **Table 1:** pH, surface areas, and quantitative analyses of ferrihydrite-hematite system during
477 transformation under alkaline conditions. Aqueous and solid As concentrations during this
478 transformation are also listed.
479

Sample ID (day)	pH	Surface area (m^2/g)	% transform XRD	% transform BET	As (aq) (mg/L)	As/Fe (molar ratios)
0	10.03	241	0	0	1.48	0.016
2	9.03*	NA	5	NA	2.28	NA
3	9.57*	204	7	15	1.92	NA
4	9.85	NA	14	NA	1.81	NA
5	9.88	194	24	20	1.54	NA
6	10.10	168	38	30	1.11	NA
7	10.56	112	55	54	0.51	0.018

480 * 0.01 M NaOH added to increase the pH to ~10.

481 **Table 2:** Arsenic K-edge EXAFS curve-fitting results summarizing the local coordination
482 environment around the arsenic atom on day 0 (arsenate adsorbed on ferrihydrite) and day 7
483 (arsenate incorporated into hematite) as well that of arsenate adsorbed on ferrihydrite and
484 scorodite. Per atom amplitude and phase parameters for fitting adsorbed arsenate were obtained
485 from mineral angelellite [$Fe^{3+}{}_4O_3(AsO_4)_2$]. The fitting was done over the k-range of 3-13$Å^{-1}$ and
486 R-range of 1-4 Å using the Hanning window in both cases.
487

	CN	R (Å)	σ^2($Å^2$)	ΔE_0 (eV)	R-Factor
Day 0					
As–O	4.0*	1.69	0.0029	7.52	0.026
As–Fe	2.0	3.27	0.0061	**	
Day 7					
As–O	4.0*	1.69	0.0031	5.41	0.031
As–Fe1	1.1	2.83	0.0048	**	
As–Fe2	1.9	3.36	0.0066	**	
As–Hematite					
As–O	4.0*	1.69	0.0027	2.99	0.023
As–Fe	0.9	2.84	0.0047	**	
Scorodite					
As–O	4.0*	1.68	0.0041	3.55	0.021
As–Fe	4.0	3.35	0.0069	**	

488 Amplitude reduction factor was constrained to 0.9. R, Interatomic distance (± 0.02Å)
489 CN, Coordination number (± 20%). σ^2, Debye–Waller factor (disorder parameter)
490 *constrained value ** value was constrained to the 1st shell
491

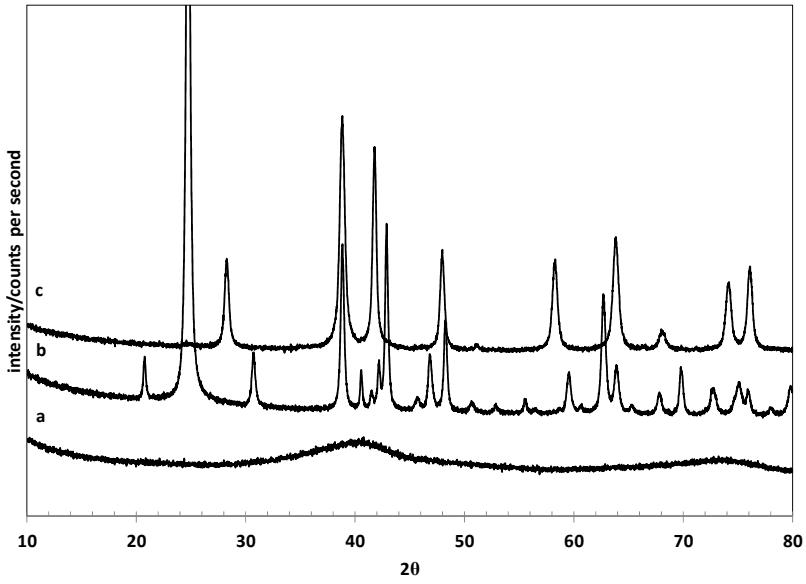

492

493 **Fig.1**

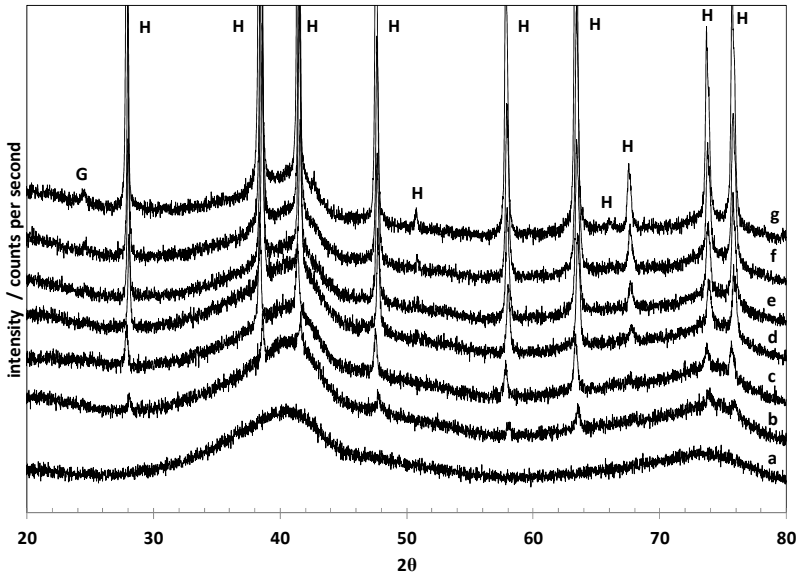

494

495 **Fig. 2**

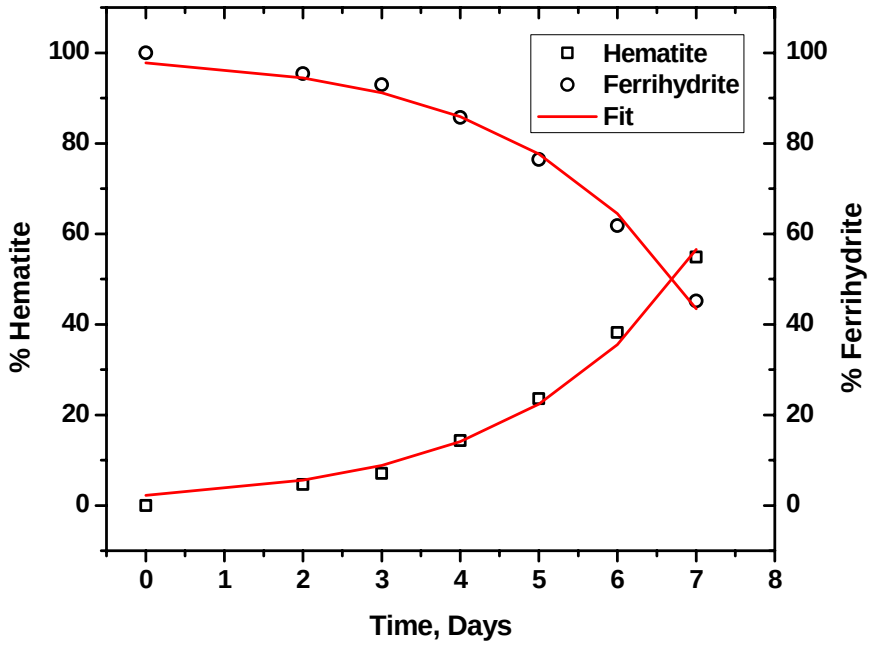

496

497 **Fig. 3**

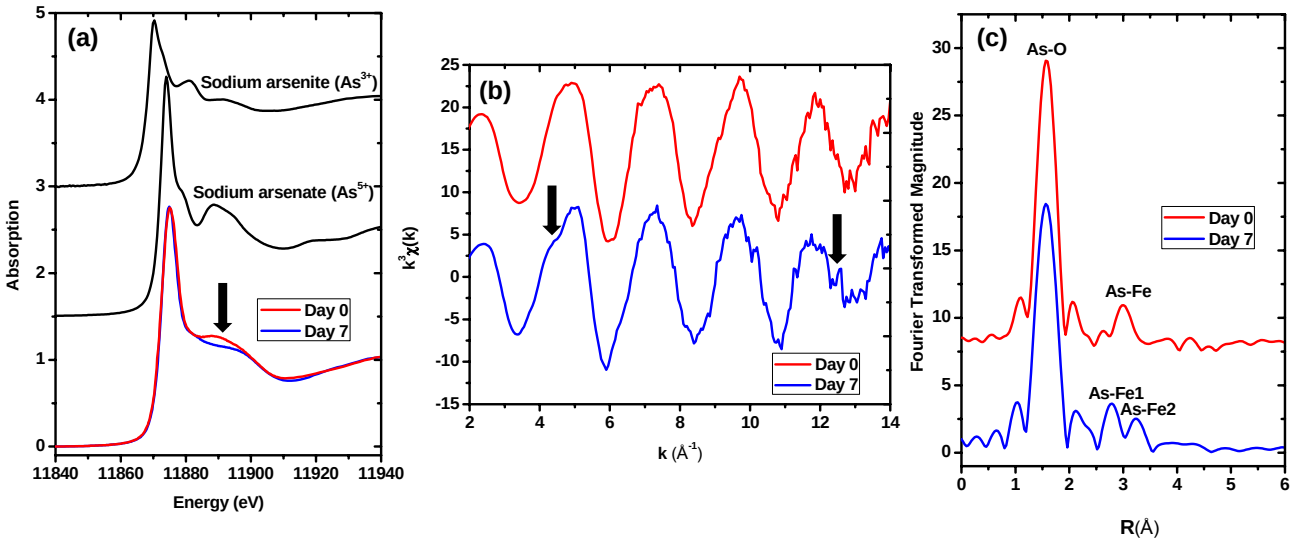

498

499 **Fig. 4**

500

501

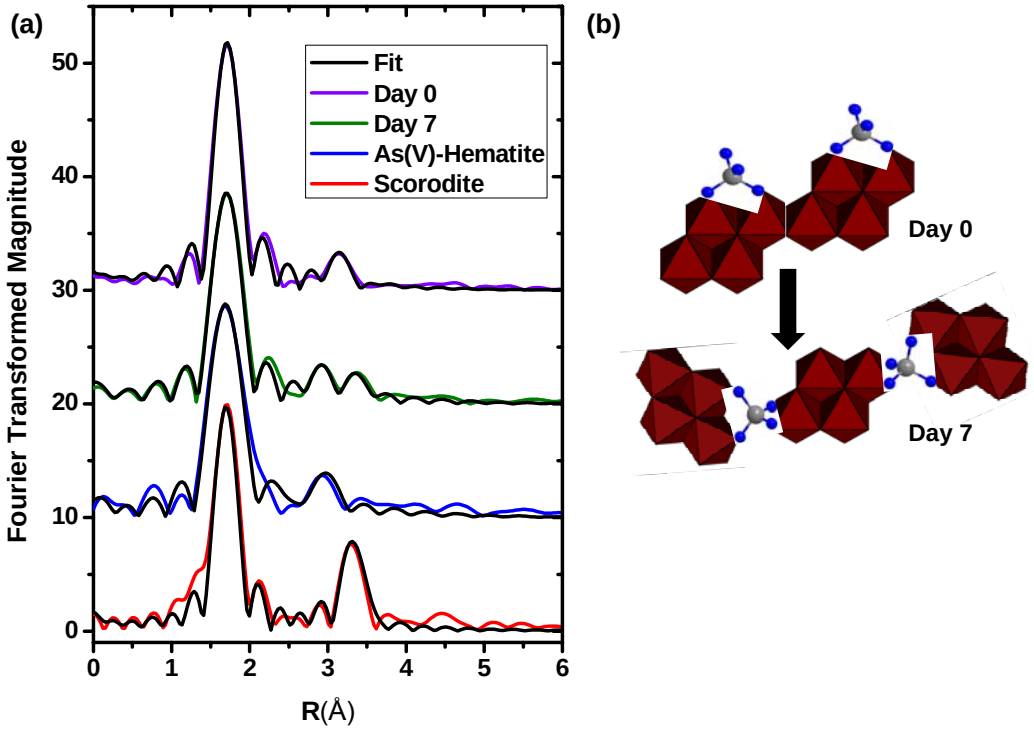

Fig. 5